SCIENCE CHINA
Earth Sciences

• RESEARCH PAPER •

March 2015 Vol.58 No.3: 329–344
doi: 10.1007/s11430-014-4924-2

Observation analysis on characteristics of formation, evolution and transition of a long-lasting severe fog and haze episode in North China

GUO LiJun[1,2], GUO XueLiang[1*], FANG ChunGang[1] & ZHU ShiChao[1,2]

[1] *Key Laboratory for Cloud Physic, Chinese Academy of Meteorological Sciences, Beijing 100081, China;*
[2] *School of Atmospheric Physics, Nanjing University of Information Science & Technology, Nanjing 210044, China*

Received November 19, 2013; accepted May 29, 2014; published online November 5, 2014

An unusual fog and haze event lasted for one week took place during 1–7 December, 2011 over North China. To investigate the characteristics and mechanism of formation, evolution, and transition of the fog and haze event, we studied the microphysical properties such as aerosol, cloud condensation nuclei (CCN), fog droplet spectrum and liquid water content (LWC), as well as horizontal visibility and boundary layer properties, using the data collected in the Project of Low-Visibility Weather Monitoring and Forecasting in the Beijing-Tianjin region. The results indicate that the long-lasting fog and haze event occurred in a high pressure weather system and calm wind condition. The stable boundary-layer structure resulted from temperature inversions that were built by warm advection and radiation cooling provided a favorable condition for the accumulation of polluted aerosols and the formation and development of the fog and haze event. In particular, the continuous southerly wet flow advection made the process a persistent and long-lasting event. The horizontal visibility was almost below 2 km in the whole process, and the lowest visibility was only 56 m. The average LWC was about 10^{-3} g m^{-3}, and the maximum LWC reached 0.16 g m^{-3}. The aerosol number concentration was more than 10000 cm^{-3}, and its mass concentration ranged from 50 to 160 μg m^{-3}. The further study shows that the fog and haze event experienced three main processes in different intensities during the whole period, each process could be divided into three main stages: aerosol accumulation, transition and mixture of aerosol and fog, and dissipation. Each stage had different physical features: the aerosol accumulation stage was characterized by the increase of aerosol number concentration in Aitken nuclei and accumulation mode sequentially. In the transition and mixing stage of fog and haze, the latent heating produced by fog droplet condensation process and high aerosol number concentration condition intensified the Brownian coagulation process, which induced the small size of aerosols to become larger ones and enhanced the CCN activation process, thereby promoting the explosive development of the fog event. The ratio of aerosol activated to CCN reached 17%, and the ratio of CCN converted to fog droplet exceeded 100%, showing an explosively broadening of fog droplet spectrum. The decrease and dissipation of the fog was caused by an increased solar radiation heating or the passage of cold frontal system.

haze and fog, aerosol accumulation, transition of haze into fog, North China

Citation: Guo L J, Guo X L, Fang C G, et al. 2015. Observation analysis on characteristics of formation, evolution and transition of a long-lasting severe fog and haze episode in North China. Science China: Earth Sciences, 58: 329−344, doi: 10.1007/s11430-014-4924-2

With the rapid urbanization and industrialization in China, the frequency and intensity of haze and fog event have shown an increasing trend in recent years, which has caused great concerns. Low visibility weather usually occurs in the stable boundary layer and is caused by the attenuation of fog and haze particles for visible light (Pinnick et al., 1978).

*Corresponding author (email: guoxl@mail.iap.ac.cn)

In the clean air condition, fog particles are composed purely of water drops or ice crystals, and have more impact on transportation than human health. But in the polluted air conditions, the coexistence of haze and fog particles can be greatly harmful to human health and ecological environment besides transportation; for example, the well-known severe fog and haze event that lasted for four days occurred in London in the winter of 1952, which was believed to cause deaths of about 4000 people. Since then, the haze and fog event has been of worldwide concern.

Since the fog and haze are different in nature, most researchers usually investigate them independently, focusing on their physical and chemical properties, and formation mechanism. The formation and prediction for different kinds of fog events have been investigated by many researchers (e.g., Gultepe et al., 2007; Niu et al., 2010), including radiation fog (Gerber, 1981), advection fog (Liu et al., 2010; Pu et al., 2008), frontal fog (Stewart, 1995), sea fog (Lewis et al., 2003), and terrain fog (Li et al., 1994). The meteorological elements, boundary layer structure, synoptic causes, and geographical conditions in which fog forms have been investigated. The fog droplet number concentration, liquid water content, fog droplet spectrum and its broadening were also explored (Li et al., 2011a). Besides, the chemical composition in the fog water is an important factor in discovering the activation ability of hygroscopic aerosols to convert into fog droplets as moisture increased (Fahey et al., 2005).

Physical properties of haze aerosols mainly include nucleation, coagulation, sedimentation, cloud scavenging, and removal processes (Husar et al., 1984) and extinction characteristics (Yu et al., 2011). Chemical composition and its properties of haze aerosols have been found to closely associate with radiative effect in climate change, air quality, and chemical reactions among gaseous, liquid, and solid phases (Heintzenberg, 1989). The haze weather event was also closely associated with anthropogenic and industrial polluted sources and synoptic situation (Stein et al., 2003; Wu et al., 2005). Liu et al. (2013) studied the formation and evolution mechanism of haze weather events in Beijing and found the primary reasons were that stable anti-cyclonic at surface, lowering of the height of planetary boundary layer, heavy pollution emissions from urban area, number and size of evolution of aerosols, and hygroscopic growth for aerosol scattering.

The haze aerosols can be transformed to fog droplets under certain conditions. The classical Köhler curve suggested that hygroscopic aerosols can become haze droplet before the saturation reaches the critical supersaturation S_c, and when the environmental saturation is equal or larger than S_c, the aerosol particles can be activated spontaneously, and the activation ability of aerosols to cloud condensation nuclei (CCN) is closely related to the size and chemical composition of aerosols (Kőhler, 1936). Eldridge (1969) suggested that the haze was transformed to fog when the visibility ranged from 500 to 1000 m. Meyer et al. (1980) found that in the transition process from haze to fog there is discontinuous and dramatic change in the relationship between visibility and aerosol number concentration when visibility falls from 2.1 to 1.4 km. The haze aerosols larger than 1 μm were activated to form fog droplets while those between 0.3 and 1.0 μm remained the constant nearly throughout the life cycle of fog. Elias (2009) classified the weather into clear, haze, and fog based on their attenuation contributions when investigating the haze and fog events in Paris, and suggested that the haze was transforming to fog when the visibility was falling from 880 to 400 m.

Some studies have shown that the properties of haze aerosols could have important effects on fog microphysics, in particular, the size distribution of fog droplets (e.g., Hudson, 1980). Ogren et al. (1992) found in Po Valley experiment fog events that the dominant fog droplets with size at or above 20 μm represented the activated aerosols, whereas the mode below 10 μm was associated with the aerosols that have grown considerably but not enough to activate. Podzimek (1997, 1998) used the impactor technique to sample the number concentration and size distribution of fog and haze droplets in different polluted places, and classified them into several types with different typical spectral shape and parameters on the basis of the width and asymmetry. Yang et al. (2010) analyzed a fog and haze event in winter of Nanjing and divided the fog and haze event into stages of haze, wet haze, mist, and fog on the basis of the visibility, relative humidity, and liquid water content, and investigated the microphysical properties such as coarse and fine particles concentration and size distribution at each stage.

The haze and fog may interact with each other when coexisting in atmosphere. On one hand, the accumulation of haze aerosols provides a significant source of CCN for fog formation, and at the same time the radiative property of haze aerosols may influence the development of fog. On the other hand, fog liquid water provides a medium for aerosol aqueous-phase chemical reactions and changes the nature and chemical properties of aerosols (Pandis et al., 1990). The secondary aerosols of sulfate and nitrate could be continuously formed and grown in the haze weather as the moisture increased (Wang et al., 2012). Nitrate could exist in a liquid state in a fog event in London (Dall'Osto et al., 2009). The reduction of SO_2 was consistent with the increase of LWC in a severe haze and fog event over the northern China (Zhang et al., 2013), which was related to the heterogeneous chemical reaction between gas and liquid.

Therefore, the formation and reaction processes of fog and haze are very complex. The identification and prediction of fog and haze event is still quite difficult due to the limitation of conventional meteorological stations. The World Meteorological Organization (WMO) used the horizontal visibility to define fog and haze. The visibility below 1 km was defined as fog and that between 1 km and 5 km was defined as light fog or haze (WMO, 2005). The defini-

tion cannot clearly identify the fog and haze when they coexist under polluted conditions. UK Met Office (UKMO) used the Relative Humidity (RH) as a criterion to identify fog and haze. The fog is with RH 100%, mist with RH between 95% and 100%, and haze with RH smaller than 95% (UKMO, 1994). China Meteorological Administration (CMA) set a classification standard involving horizontal visibility, RH, and aerosol mass concentration and its scattering and absorption coefficient for fog and haze event (CMA, 2003, 2010), but it is hard to apply in operational meteorological service due to that most of meteorological stations have no observations for atmospheric aerosols, hence most stations still use the horizontal visibility and RH as classification standard for fog and haze.

In addition, the previous research results about the effect of haze aerosols on fog were not consistent: some studies showed that the increase of haze aerosols could strengthen the fog formation and development (Jia et al., 2012), and other studies showed that the radiation effect induced by haze aerosols could lead to the reduction of fog occurrence in frequency (Gautam et al., 2007).

In recent years, the fog and haze events take place frequently in northern China; however, the transition and interaction effect of fog and haze are not well investigated. This study investigates the characteristics of formation, evolution, and transition of a long-lasting severe fog and haze event in northern China by using the data collected by the observation platform of fog and haze of Chinese Academy of Meteorological Sciences. The microphysical properties are explored, such as aerosols, cloud droplet condensation nuclei, fog droplet spectrum, and liquid water content as well as the features of atmosphere visibility and boundary-layer structure that the fog formed. The characteristics and mechanism of haze aerosols accumulation and the transition from haze to fog are particularly emphasized in this study in order to provide more scientific evidence for identification and prediction of haze and fog event.

1 Instruments and field observations

The comprehensive field observation is located in the Zhuozhou Meteorological Bureau (39.48°N and 115.97°E) of Hebei Province south of Beijing. The advanced observation instruments include fog monitor, scanning mobility particle sizer, CCN counter, visibility sensor, multi-channel ground-based microwave radiometer, and tethered balloon sounding system. The instruments and their specifications are listed in the Table 1.

The meteorological data from Micaps are used for analyzing synoptic systems. MODIS visible cloud image, cloud and aerosol products are the significant information to identify and estimate horizontal distribution of fog and haze.

2 Results

2.1 Characteristics of synoptic system and boundary-layer structure of the fog and haze event

The formation and evolution of the unusual low-visibility fog and haze event lasted for one week was closely associated with the variation of the complicated synoptic systems. On 1 December, 2011, the whole northern China was controlled by a surface high pressure system, and then controlled by a surface low-pressure system on 2 December. The intermittent light snow and fog weather were recorded at 08∶00 and 20∶00 (Beijing Time, the same hereafter) on 2 December by Beijing Meteorological Station. Northern China was dominated by the surface high pressure system again at about 08∶00 on 3 December. Due to the influence of a weak cold front from northwest, the weather became clear until night. The intensive radiative cooling on the ground resulted in another process of fog and low-visibility event in the early morning on 4 December, and the wind at 850 hPa turned southwesterly at about 08∶00. The water

Table 1 Instruments used in the field observation of fog and haze

Instrument	Parameter	Range and resolution	Frequency
Fog Monitor-100 (FM-100) (DMT)	Fog droplet number concentration, size distribution, LWC	2–50 μm, 20 bins	1 s
Scanning Mobility Particle Sizer-3936 (SMPS-3936) (TSI)	Aerosol number concentration and size distribution	0.015–0.661 μm, 106 bins	3–4 min
Cloud Condensation Nuclei Counter (CCNC-100) (DMT)	CCN number concentration	0.75–10 μm, 21 bins	1 s
Microwave Radiometer MP-3055A (MWR) (Radiometrics)	Profiles of temperature, relative humidity, water vapor content and LWC	Inversion data, not direct detecting data	2–3 min
Visibility Sensors PWD20 (Vaisala)	Horizontal visibility distance	Range: 0–2000 m; resolution: 1 m	1 min
Sounding Balloon XLS-II (Institute of Atmospheric Physics)	Profiles of temperature, relative humidity and wind	Resolution: 0.1°C, 0.1%, 0.1°, 0.1 m s^{-1}	1 min
Laser Precipitation Monitor (LPM-5) (Thies Clima)	Rainfall intensity and phase state from fall speed and sizes of particles detected directly based on algorithm	Resolution of rainfall intensity: 0.001 mm h^{-1}	1 min
Automatic Meteorological Station-CAWS600B (Huayun Group)	Temperature, pressure, relative humidity, and wind at surface, vapor pressure and one-minute accumulated precipitation	Resolution: 0.1°C, 0.1 hPa, 1%, 1°, 0.1 m s^{-1}, 0.1 hPa, 1 mm	1 min

vapor was persistently supplied from southwest on 5 December. The fog and haze event continued with some oscillations and was finally terminated by a strong cold front from northwest.

Figure 1 shows the temporal evolutions of surface meteorological factors in the whole fog and haze process at Zhuozhou meteorological station. Both cold and warm fog occurred at different stages of the fog and haze event associated with the variation of temperature T and RH (Figure 1(a)). The cold fog occurred with T smaller than 0°C on 4–5 December, and then became warm fog with the increase of T due to the warm and wet airflow after 5 December. RH remained above 90% through the whole fog and haze process and even reached 100% when the vapor saturated during the formation and development of fog. RH varies with T reversely, the high RH corresponded low T, and low RH corresponded high T. The fog formation and development in the evening on 3 December and in the morning on 4 December were attributed mainly to the increase of RH and decrease of T.

Figure 1(b) shows the temporal variations of surface pressure, vapor pressure, and one-minute accumulated precipitation. The surface pressure started to drop from 1 December, and then slowly ascended again. The corresponding vapor pressure increased steadily and then remained at a high value until the dissipation of the fog and haze event. Two evident precipitations occurred at about 11∶00 on 2 and 5 December in the fog and haze period.

Figure 1(c) shows the wind speed and direction averaged in 10 min. The wind speed at surface was about 1–2 m s^{-1}. The main reason for the formation of the long-lasting fog and haze event was due to the stable stratification and calm weather conditions controlled by a surface high pressure system, which was not favorable to the diffusion and dissipation of haze aerosols and fog. The surface wind direction tended to change largely due to the effect from complex land surface. The southerly wind prevailed before 5 December and from the afternoon to the night of 6 December. Therefore, the weak or calm wind was conducive to the development and persistence of the fog and haze event, and the different directional airflow brought dry or wet air mass, which produced strong and weak variations of the event. The fog and haze event was dissipated by a strong cold front started from the noon of 7 December. Thus, the synoptic cause for the fog and haze event was due to a persistently stable, calm and highly humid atmospheric environment formed in northern China, and the radiation cooling and polluted aerosol accumulation directly produced and maintained the event.

Fog and haze occurs within the boundary layer. To reveal the vertical structures of temperature, humidity, and wind at the boundary layer where the fog and haze episode occurred, a sounding balloon was used during the days on 2–5 December. The profiles of temperature, RH, and wind are displayed in Figure 2. Due to the precision limitation of the sounding humidity probe, the maximum RH from sounding

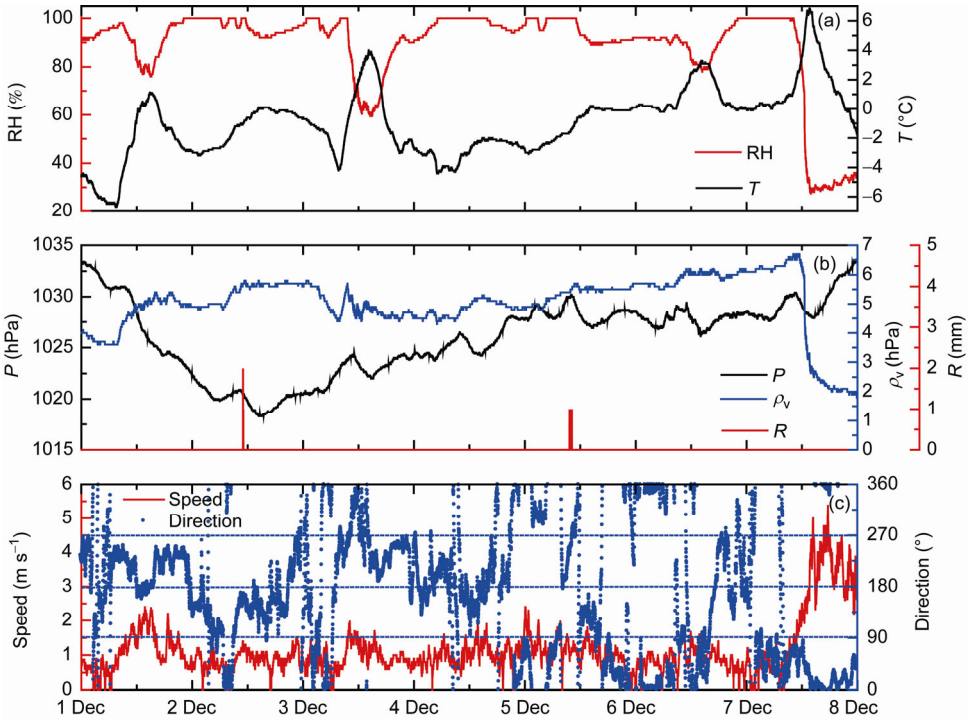

Figure 1 Temporal variations of surface meteorological factors in the whole fog and haze process at Zhuozhou Meteorological Station. (a) Relative humidity RH (red curve) and temperature T (black curve); (b) surface pressure P (black curve), vapor pressure ρ_v (blue curve) and 1-min accumulated precipitation R (red column); (c) wind direction (blue scatters) and speed (red curve).

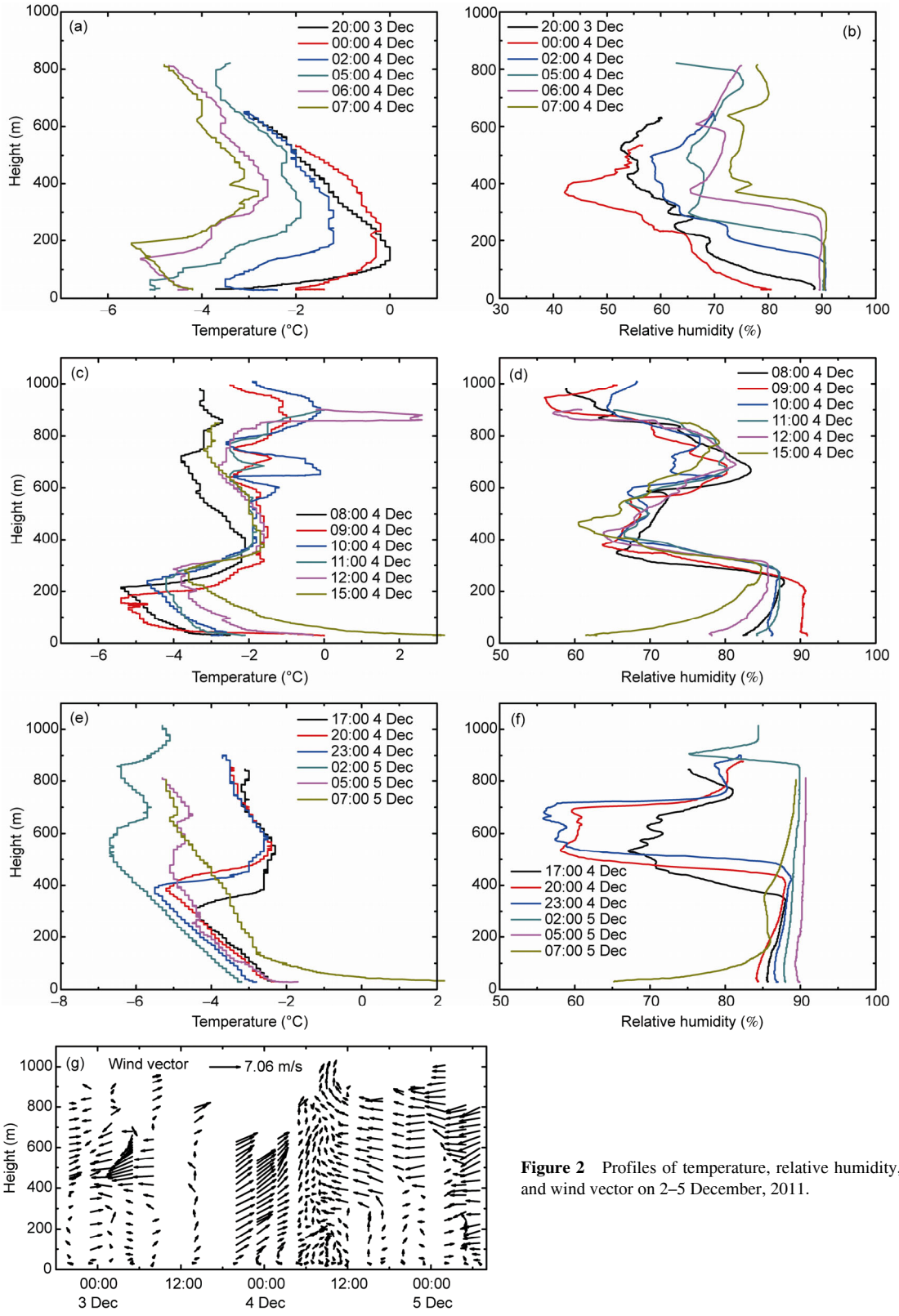

Figure 2 Profiles of temperature, relative humidity, and wind vector on 2–5 December, 2011.

balloon only reached 90%, but the corresponding RH at surface meteorological station reached 100%. In order to correct the observation of sounding humidity probe, the RH value of 90% in sounding humidity probe was regarded as 100%.

The temperature profiles at nighttime from 20∶00 on 3 December to 07∶00 on 4 December are shown in Figure 2(a). It shows that the temperature tended to decrease due to

longwave radiation cooling at nighttime and a strong inversion layer with cooling rate of 3°C (150 m)$^{-1}$ has formed by 20∶00 at near surface, which was conducive to the accumulation of aerosols and water vapor. The cooling process persisted and the temperature decrease reached its maximum until 05∶00 on 4 December, and the fog showed an explosive development at this time, the thickness of temperature inversion reached 300 m, and the maximum RH reached about 200 m where is the fog top height. From 06∶00, the heating from solar shortwave radiation increased and surface temperature tended to increase. The surface radiation cooling at nighttime induced the increase of relative humidity at the same time (Figure 2(b)). The southwest weak airflow predominated at high-levels until 07∶00 (Figure 2(g)) and provided weak moisture supply. The fog top height reached more than 300 m.

The temperature and humidity profiles at daytime from 08∶00 to 15∶00 on 4 December are shown in Figure 2(c) and (d). At daytime, the surface temperature started to increase due to the shortwave radiation warming after sunrise. The weak southwesterly wind tended to turn into southeasterly wind and further developed from 09∶00 (Figure 2(g)), and produced double temperature inversion layers at 200–400 and 700–900 m (Figure 2(c)). The high RH was maintained primarily below 300 m. However, another humidity inversion layer between 400–800 m was produced due to the influence of weak southeasterly moisture airflow above 300 m. Although the fog tended to weaken due to the effect of solar radiation warming at daytime, it did not dissipate completely. The main reason for it can be attributed to the formation of deep double temperature and humidity inversion structure.

The temperature and humidity profiles at nighttime from 17∶00 on 4 December to 07∶00 on 5 December are shown in Figure 2(e) and (f). The temperature inversion structure at 400–600 m tended to weaken from 23∶00 on 4 December and disappeared in the early morning on 5 December. However, RH still maintained its maximum and tended to extend to higher levels, and the fog top height reached about 900 m. This is due to that the stronger cold advection induced by northeasterly wind provided a favorable condition for vapor condensation process and fog formation (Figure 2(g)). Therefore, the radiation fog turned into advection fog from 5 December. Moreover, the ascending fog continued to develop and produced drizzle at surface. The drizzle rainfall was recorded by the local automated meteorological station and Laser Precipitation Monitor (LPM-5) at about 10∶00.

The structure and evolution of temperature and relative humidity at boundary layer obtained from sounding balloon are basically consistent with that retrieved from MWR (Figure 3). For example, the temperature inversion structure from the night on 3 December to the early morning on 4 December, and also the transition from radiation fog to advection fog on 5 December. However, the retrieved data of MWR are less precise than those of sounding balloon in some aspects. MWR uses passive remote sensing way to obtain profiles of *T*, RH, and LWC based on neural network algorithm with past sounding data and bright temperature as input, which is different from direct observation of sounding balloon. In addition, the vertical resolution of MWR is only 100 m for the height between 500 and 2000 m, which is not enough to obtain the fine structure of the upper boundary layer. But MWR has higher temporal resolution, so that it is still very useful compared with conventional radiosonde observation, which only has observation twice a day.

2.2 Microphysical properties of the fog and haze event

Fog is usually regarded as cloud at surface, and it has much weaker updraft, vertical temperature gradient, and supersaturation than cloud. Radiation fog is induced by radiation

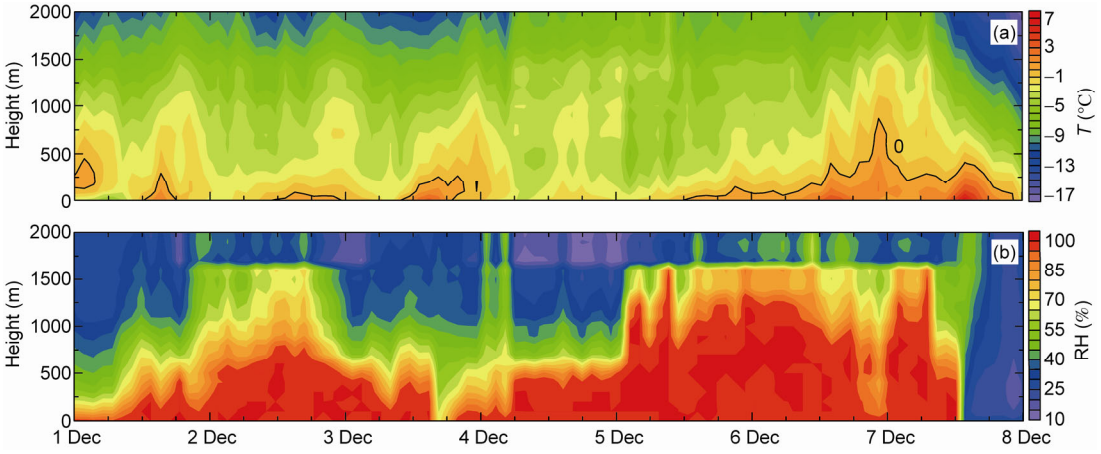

Figure 3 Time-height distributions of temperature and relative humidity from MWR on 1–7 December, 2011. (a) Temperature (The black curve is the isotherm at 0°C); (b) relative humidity.

cooling. In polluted regions, there are higher polluted aerosols during foggy days, so that the generation and development of fog is closely relevant to CCN formed from polluted aerosols.

Figure 4(a) shows the Terra-MODIS visible cloud image at 10∶50 on 4 December. It shows that the northwestern region in Beijing City and Hebei Province had less cloud due to the passage of cold front from 3 December. The fog top temperature for radiation fog should be nearer to the ground temperature, or even slightly higher than ground temperature due to the effect of temperature inversion. The advection fog is usually accompanied by low and middle clouds, so the cloud top temperature might be lower than fog top temperature. Combining with the distribution of cloud top temperature in Figure 4(b), we may identify the fog formation region from satellite data. Figure 4(a) and (b) indicates that the radiation fog at 10∶50 on 4 December mainly covered southeastern Beijing and eastern Hebei, and the sea fog was distributed along the southern Bohai gulf. The Micaps data show that the fog also occurred in southeastern Hebei, which might be advection fog based on the distribution of cloud top temperature. Figure 4(c) and (d) presents the distributions of aerosol optical depth (AOD) and Angstrom exponent in the cloudless region. AOD was almost less than 0.4 in the north of Hebei, and up to 1.0 around the Bohai Gulf. Although the AOD retrieval is limited in cloudy area due to cloud effect, it should be inferred that the aerosol concentration was much higher in cloudy area. Angstrom exponent was approximately 2 in northern Beijing and eastern Heibei and the sporadic high values of AOD existed over Beijing area, indicating the very fine aerosols particles existed in these regions (Remer et al., 2006). Therefore, the foggy regions were distributed primarily in the most regions of Beijing and southeastern Hebei, and the size of aerosols in the cloudless area in northern Beijing and eastern Hebei was very small, indicating that it was a weather event with fog and haze coexisted.

Figure 5(a) shows that the horizontal visibility L was almost less than 2 km and had apparent fluctuations during the period of fog and haze episode. Based on the grade standard of visibility for fog or haze of CMA (CMA, 2003, 2010), the visibility on 1 December was located mainly between 1 and 2 km, it should be regarded as severe haze weather, and from 18∶00 on 1 December to 09∶00 on 3 December, the L was between 0.5 and 1 km, it should be regarded as fog weather. L started to decrease sharply from 18∶00 on 3 December, and it was lower than 100 m at 05∶00–08∶00 on 4 December and the lowest L was 56 m. It should be regarded as dense fog. In the later stage from 5 December to 18∶00 on 6 December, L fluctuated around 1 km and then reached at 500 m from 18∶00 on 6 December to the noon on 7 December. After that, L increased rapidly

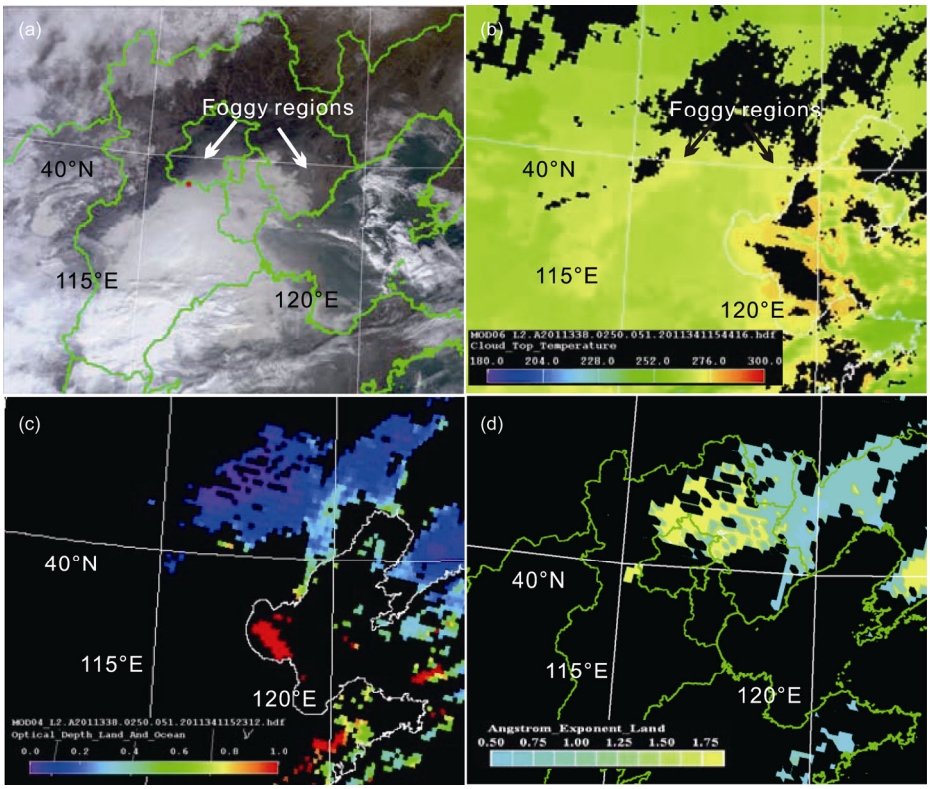

Figure 4 MODIS visible image (a), cloud top temperature (b), aerosol optical depth (c) and Angstrom exponent (d) over land at 10∶50 on 4 December. Red dot is the observation site in Figure 4(a).

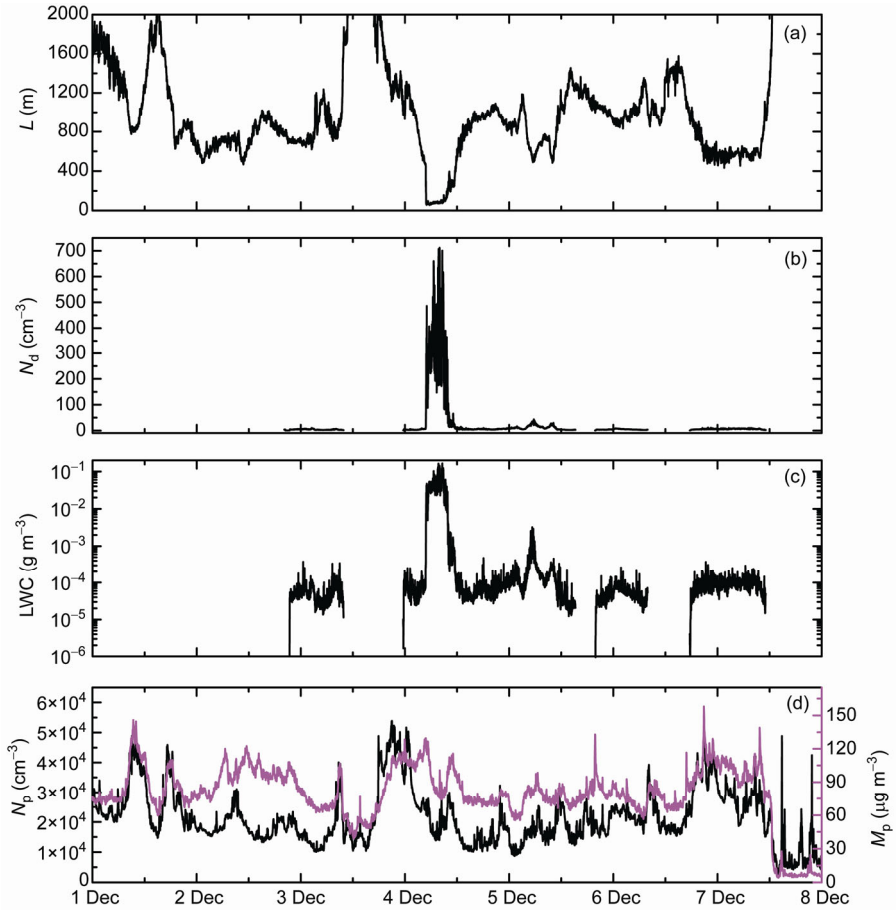

Figure 5 Temporal variations of physical parameters of the fog-haze process on 1–7 December, 2011. (a) Horizontal visibility L; (b) fog droplet number concentration N_d; (c) LWC; (d) aerosol number concentration N_p (black curve) and mass concentration M_p (pink curve). Aerosol parameters are averaged in 3 min, and others are averaged in 1 min.

and the fog and haze event dissipated.

Fog droplet number concentration (N_d) and liquid water content (LWC) also had distinct characteristics in temporal variations (Figure 5(b) and (c)). Both N_d and LWC reached their highest values at 05∶00–08∶00 on 4 December, and additional two peaks occurred in the morning on 5 December. LWC was more than 10^{-4} g m^{-3} when RH reached 100% at surface, and it was in order of 10^{-5} g m^{-3} at other periods for this episode. The N_d and LWC values were lower than those in the other dense fog study (Liu et al., 2010). The numerous haze droplets could be generated from high concentration of hygroscopic aerosols in high humidity and polluted conditions; however, the high value of LWC should be attributed to large fog droplets.

Figure 5(d) shows the temporal variations of total number concentration (N_p) and mass concentration (M_p) of aerosol particles with a size range from 0.015 to 0.661 μm. N_p reached more than 10000 cm^{-3} before the noon on 7 December, in which N_p was even more than 30000 cm^{-3} at three different periods: 1 December, from the evening on 3 December to the early morning on 4 December, and in the evening on 6 December. The results are consistent with the averaged N_p of 24000 cm^{-3} measured in fog and haze of Tianjin (Quan et al., 2011). In addition, the temporal variations of M_p and N_p were not completely consistent, such as the period from 18∶00 on 2 December to 09∶00 on 3 December. The reason will be explained later.

To further understand the characteristics of formation, evolution, and transition of the fog and haze episode, Figure 6 shows the temporal variations of vertical distributions of LWC retrieved from MWR, fog droplet size distribution from FM-100, aerosol number, and mass concentrations from SMPS. The temporal variation of LWC retrieved from MWR in Figure 6(a) is in good agreement with the number concentration of fog droplets in Figure 6(b) over the whole period of fog and haze event, indicating that the MWR can be useful and reliable to identify the evolution and development of fog. The fog size distribution in Figure 6(b) shows that the maximum size of fog droplets reached 50 μm and the number concentration was the order of 10^2 μm^{-1} cm^{-3} in the dense fog stage. However, in the mist stage the size of fog droplets was less than 20 μm. The number concentration of fog droplets was the order of 10^0–10^1 μm^{-1} cm^{-3} in the range of 2–6 μm, and contributed the half of total LWC.

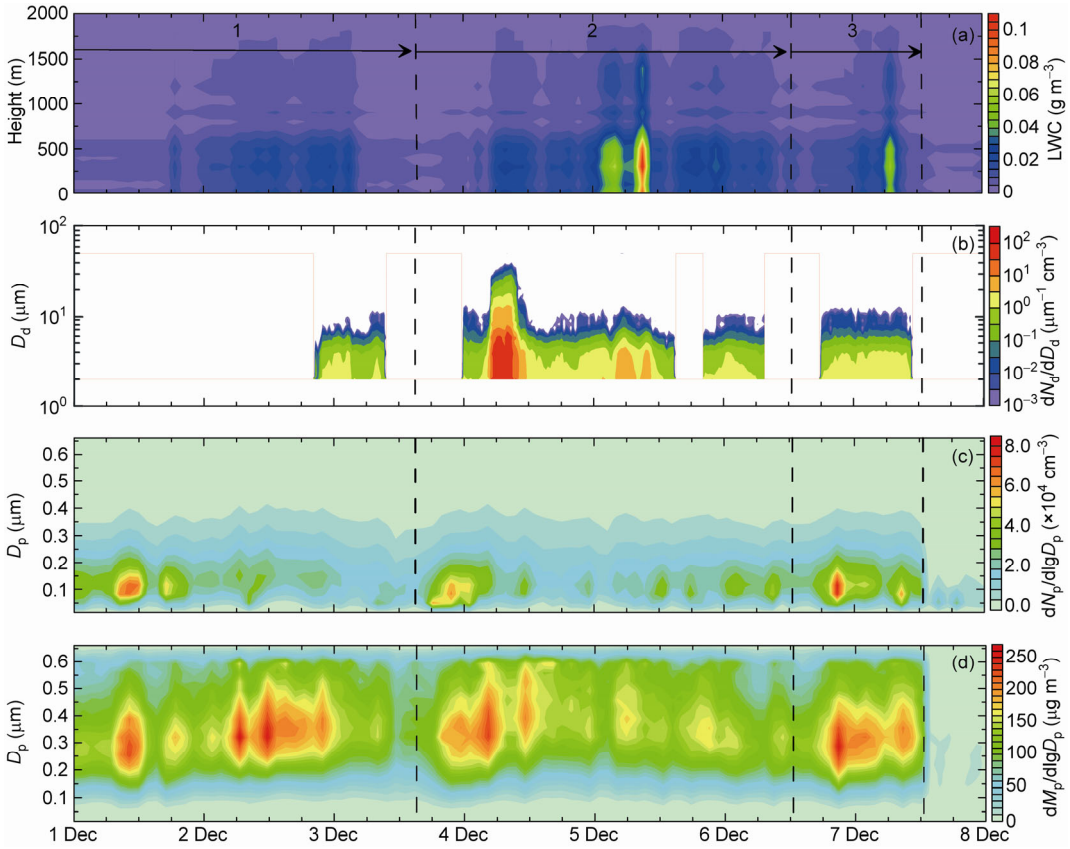

Figure 6 Time-height distributions of liquid water content retrieved from microwave radiometer (a), temporal variations and size distribution of fog droplet number concentration (b), aerosol number concentration (c), and aerosol mass concentration (d) on 1–7 December, 2011. Fog monitor was only in operation during fog period. The vertical dotted lines indicate three main processes of fog and haze episode, and corresponding number is the order of them.

The LWC was placed mainly below the height of 600 m, and the levels between 600–1500 m were affected largely by low cloud and advection. The low-visibility weather experienced three developing and weakening stages during 1–7 December based on the evolution of LWC. The two weakening stages that occurred at 08∶00 on 3 December and 12∶00 on 7 December were associated with the passage of two cold fronts. There was still higher concentration of aerosols during the weakening stage although low fog water and short duration phenomenon occurred, which led to the low-visibility event (Figure 6(c), (d)). The mass concentration of aerosols of haze weather should reach 65 μg m^{-3} for size less than 1 μm in diameter based on reference standard for haze weather (CMA, 2010). But the mass concentration of aerosols obtained from SMPS for diameter less 0.661 μm in this study almost exceeded the reference standard, indicating that the low-visibility event has the property of haze weather.

According to the observed characteristics described above, this fog and haze episode could be divided into three typical processes (Table 2). And each process had three main stages including haze aerosols accumulation, transition and mixture, and dissipation of fog and haze. Each stage had an obvious physical property.

In the stage of haze aerosols accumulation, the main features were the accumulation of aerosols, low LWC, high RH at near surface, and small aerosols whose size was less than 0.2 μm. These features were found at the daytime of 1 December and the nighttime of 3 and 6 December. The stable boundary layer induced by temperature inversion played a critical role in the accumulation of fine particles from natural and anthropogenic sources. The two temperature inversions on 1 and 3 December were related to surface longwave radiation cooling, and those on 6 December were produced primarily by the warm advection at higher levels.

The transition and mixture of fog and haze usually happened in the conditions of radiation cooling and high humidity at nighttime. Under these conditions, the aerosol mass concentration was increased by coagulation process of Brownian motion, and the increased size of aerosols was located mainly over the range of 0.2–0.55 μm, providing plenty of appropriate sizes of aerosols for condensation nucleation process of fog. When RH at surface approached 100%, haze aerosols started to convert into fog droplets, and LWC increased consequently. The processes of transition and mixture of haze and fog could not be separated clearly. When water vapor saturated, haze aerosols could be activated to form fog droplets, and the aerosols particles that

Table 2 Divisions of the fog-haze process on 1–7 December, 2011

Order	Aerosols accumulation stage	Transition and mixture stage	Dissipation stage
1	00:00 on 1 Dec–22:08 on 1 Dec	22:09 on 1 Dec–08:19 on 3 Dec	08:20 on 3 Dec–14:59 on 3 Dec
2	15:00 on 3 Dec–01:08 on 4 Dec	01:09 on 4 Dec–10:48 on 5 Dec	10:49 on 5 Dec–12:31 on 6 Dec
3	12:32 on 6 Dec–21:32 on 4 Dec	21:33 on 6 Dec–09:37 on 7 Dec	09:38 on 7 Dec–12:36 on 7 Dec

were continuously accumulated could mix and coexist with fog droplets. The mixture and transition of haze and fog could lead to the rapid decrease of visibility. The visibility L in the mixture and transition stage in the first process ranged from 0.5 to 1.0 km, that in the second process reached the lowest value of 56 m, and that in the third process was similar to the first process. The N_p and M_p in the mixture and transition stages of three processes decreased, which was induced by precipitation washout process (Figure 7). During the mature stage of haze and fog event, the accompanied drizzle and snow played an important role in wet deposition of haze aerosols. The precipitation process was consistent with the high values of LWC retrieved from MWR in the morning on 5 December, and that on 4 December derived was probably from sedimentation and freezing of large fog droplets. There was no precipitation recorded on 6 December, and the high LWC was related to the formation of dense fog.

The weakening and dissipating of the fog and haze episode are attributed mainly to the passage of cold frontal system such as that on 3 and 7 December. However, the temperature increase due to the solar radiation heating was probably the main factor for the weakening of the second haze and fog process. And the later radiation cooling at nighttime and advection of warm and wet airflow again promoted the development of fog and haze process.

The CCN had distinct features in the three stages. Figure 8 shows that temporal variation of CCN at different supersaturation (ss) of 0.2%, 0.4%, 0.6%, 0.8%, and 1.0%. Hudson (1980) studied the CCN concentration of fog droplets (ss$\leqslant$0.2%) and CCN (0.2%$\leqslant$ss$\leqslant$1.0%) in different polluted conditions, and found that CCN concentration at ss=0.2% was approximately 800 cm^{-3} with the visibility of 520 m in the one fog event of San Diego, and approximately 2000 cm^{-3} with the visibility of 380 m in another fog event under same polluted conditions. In this study, the mean CCN concentration was of the order of 10^2–10^3 cm^{-3}, and 10^4 cm^{-3} in maximum. The CCN had relatively steady continuous variation in the accumulation stage of haze aerosols, and it had a dramatic increase in the transition and mixture stage. The explosive activation of CCN corresponded well with the high LWC such as that at 12:00 on 2 December, 07:00 and 16:00 on 4 December, and provided sufficient condition for a rapid or explosive development of fog under a sharp decrease of temperature and increase of humidity conditions. The relationship between the high CCN concentration and the high aerosol number concentration was not very well, but the high CCN concentration generally corresponded well to the high aerosol mass concentration, indicating that the CCN was derived mainly from accumulation mode or larger-size aerosols. Figures 7 and 8 show that the precipitation process could block the increase of CCN and in particular, it had an apparent role in the sedimentation of accumulation mode or larger-size aerosols.

2.3 Haze aerosol accumulation, transition mechanism from haze to fog and conversion rate

To investigate the mechanism of haze aerosol accumulation and transition from haze to fog, the second process, as a representative example, will be further studied. The second process could be divided into three typical stages according to the features of LWC, RH, and aerosol concentration. The statistical characteristics for each stage are listed in detail in Table 3. Aerosols can be classified into Aitken nuclei mode with diameter D_p<0.1 μm and accumulation mode with

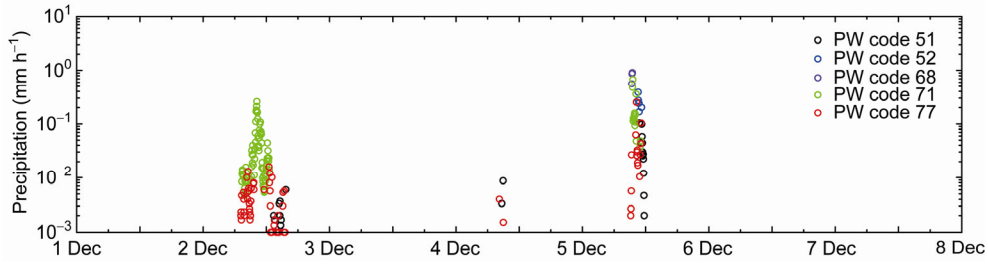

Figure 7 Temporal variations of different type precipitation intensities on 1–7 December, 2011. The data missed from 20:00 on 4 December to 09:10 on 5 December. Present weather codes 51, 52, 68, 71, and 77 represent for continuous and unfreezing drizzle, intermittent and unfreezing drizzle, slight rain or drizzle and snow, continuous falling snowflakes, and snow grains, respectively.

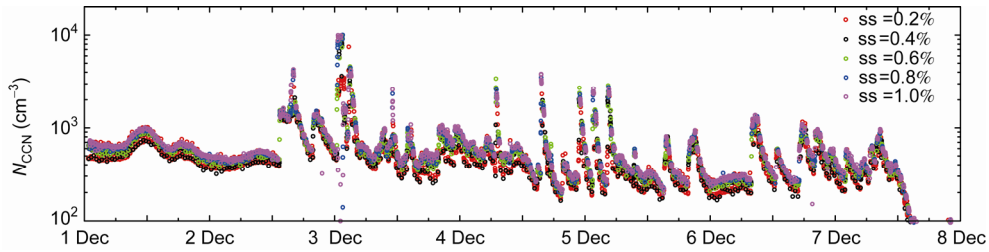

Figure 8 Temporal variations of CCN at the supersaturation (ss) of 0.2%, 0.4%, 0.6%, 0.8%, and 1.0% on 1–7 December, 2011.

Table 3 Statistical properties of some physical parameters at each stage in the second process[a)]

Stage	LWC* (g m^{-3})	N_d* (cm^{-3})	N_p* (cm^{-3})	M_p* (μg m^{-3})	Range of RH (%)	RH* (%)	Range of L (m)
Haze aerosols accumulation	7.6396×10^{-5}	3.06	36430.14	87.30	[60, 93]	82.81	⩾930
Transition and mixture	6.9069×10^{-3}	55.00	17367.40	83.07	[92,100]	98.26	[56, 1185]
Dissipation	4.7825×10^{-5}	3.84	21202.82	77.62	[81,100]	90.93	[754,1546]

a) * denotes averaged values.

diameter between 0.1 and 1.0 μm (WMO, 2003) in terms of size.

Figure 9(a) shows the temporal variations of aerosol number and mass concentrations in both modes. In the aerosol accumulation stage, the Aitken nuclei number concentration (N_p1) of aerosols increased rapidly at first, and then followed by the increase of accumulation mode (N_p2), indicating that aerosols were transited from Aitken nuclei mode to accumulation mode. Since most of Aitken nuclei are the production of secondary aerosols converted from gaseous chemicals and can form accumulation mode aerosols by physical processes of Brownian motion and turbulent coagulation (Friedlander, 2000; Tang et al., 2006). The aerosols in Aitken nuclei (M_p1) mode did not have an obvious variation in mass concentration due to their small size, and aerosols in accumulation mode (M_p2) had an apparent increase in mass concentration due to their larger size.

In the transition and mixture stage of fog and haze, at which the water vapor was saturated, some aerosols in accumulation mode could be activated as CCN and converted to fog droplets through condensation growth process, and induced the increase of LWC (Figure 9(b)). For aerosols

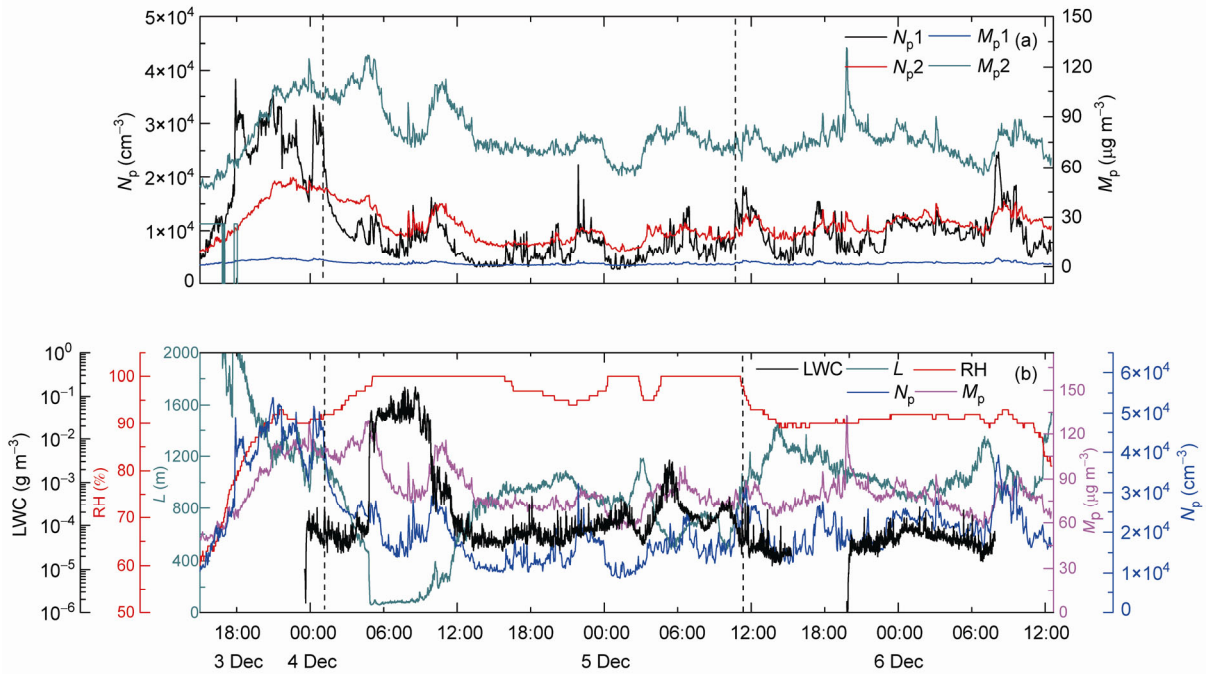

Figure 9 (a) Temporal variations of number concentration N_p1 (black curve) and mass concentration M_p1 (blue curve) of Aitken nuclei mode and N_p2 (red curve) and M_p2 (dark cyan curve) of accumulation mode in the second process; (b) temporal variations of N_p (blue curve) and M_p (pink curve) of aerosol, L (dark cyan curve) and RH (red curve) and LWC (black curve) in the second process. The vertical dotted lines indicate three typical stages including haze aerosol accumulation, transition and mixture, and dissipation of fog and haze.

with size smaller than 1 μm, the Brownian coagulation process was found to be a primary coagulation mechanism and impact and change the number and size of aerosols (Friedlander, 2000; Husar et al., 1972; Jacobson et al., 1997). The latent heat release of condensational growth of fog droplets and high aerosol number concentration condition could enhance the Brownian coagulation process, resulting in the reduction of aerosol concentration in Aitken nuclei mode. In the beginning period of fog formation, the aerosol mass concentration in accumulation mode increased, and the reason for it is complex. Although under unstable stratification condition the aerosol mass transformed from Aitken nuclei mode to accumulation mode through Brownian coagulation process is usually weak, and under stable condition the continuous accumulation of aerosols from emission sources might make the mass transformation obvious. In addition, the gas-particle transformation might also be an important factor; for instance, SO_2 can be oxidized through a series of reactions to generate sulfate acid, and with ammonia and water vapor the sulfate acid can be converted into ammonium sulfate, and it is similar to sulfate (Seinfeld et al., 1997; Drewnick et al., 2004). After the formation of fog droplets, the part of aerosols in accumulation mode can be removed through wet scavenging and washout processes, reducing aerosols in accumulation mode.

The fog experienced an explosive development. From 04∶45 to 04∶58 on 4 December, the LWC increased from 10^{-5} to 10^{-2} g m^{-3}, and the visibility dropped from 467 to 59 m. The visibility was lower than 100 m from 05∶00 to 08∶00 on 4 December. During the explosive developing stage, a large number of aerosols in accumulation mode were transformed into fog droplets and fell to the surface by wet deposition process. Therefore, the aerosol number and mass concentration decreased obviously in this period. This could also be verified by data from LPM-5. The decrease of aerosol number and mass concentration occurred for periods of 05∶00–10∶00 on 4 December and 00∶00–05∶00 and 09∶00–11∶00 on 5 December. The first decrease was caused mainly by washout of fog droplets, and the second and third reductions in N_p and M_p corresponded well to the high values of LWC derived from MWR. The LPM-5 data were unavailable in the second decrease and could not be used to illustrate the precipitation type. In the third reduction course, the precipitation particles transformed from snow grains to drizzles and the precipitation process had an apparent wet removal effect on haze aerosols. After the explosive development stage, the fog tended to weaken and sustain. In an open space, the aerosols were continuously input, formed, and transformed, and the N_p and M_p were kept in a relatively stable variation state though there were some oscillations. The transition and mixture stage lasted for about 30 hours and the averaged LWC reached over an order of 10^{-3} g m^{-3}. In the dissipating stage, although the LWC decreased dramatically, the N_p and M_p of haze aerosols did not vary significantly, indicating that the mist and haze dominated the stage.

The time series of aerosol number and mass concentration shown in Figure 10 indicated that in the haze aerosols accumulation stage, the peak of aerosol number concentration was transformed from 0.04 μm at Aitken nuclei mode to 0.11 μm at accumulation mode, and resulted in the change of aerosol size distribution, which was induced possibly by Brownian coagulation process. The wedge type of high aerosol number concentration was consistent with the high value between 0.02–0.2 μm obtained in Nanjing (Kang et al., 2013), and also with the banana-shaped type in Beijing (Liu et al., 2013). The coagulation process of haze aerosols happened at size below 0.5 μm (Husar et al., 1984), and in particular, the reduction of aerosols particles less than 0.2 μm during the transition and mixture of fog and haze was caused primarily by coagulation process (Jacobson et al., 1997), during which the mass concentration of

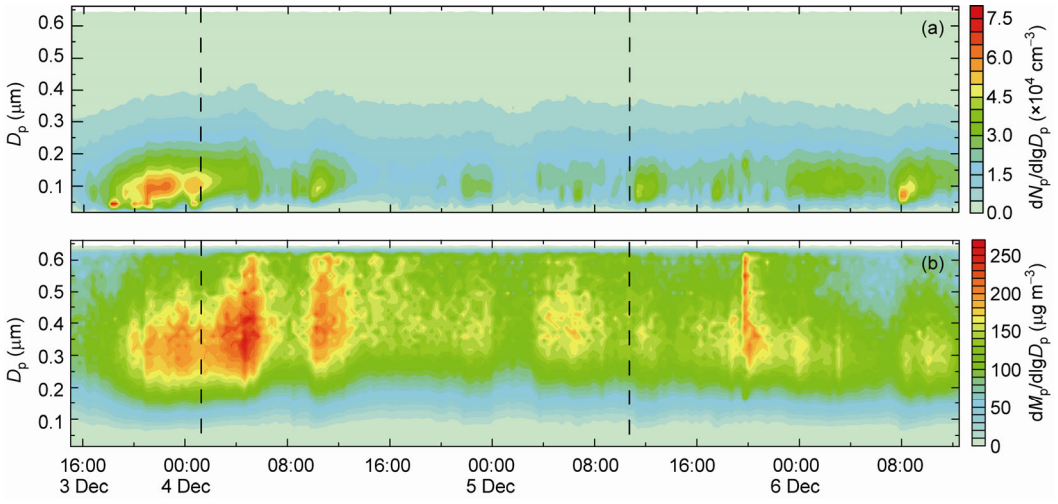

Figure 10 Temporal variations of size distributions of aerosol number concentration (a) and aerosol mass concentration in the second process (b).

aerosols rapidly increased and was distributed mainly in diameter between 0.2 and 0.55 μm. The characteristics were in good agreement with the size distribution of organic, sulfate, nitrate, and ammonium (Drewnick et al., 2004).

The aerosol chemical composition, diameter, and water vapor saturation are important factors to influence the activation ratio of aerosols. When the environment reaches a critical supersaturation condition required for one size of aerosol, the aerosol particle can be activated spontaneously, and the larger the particle, the easier the activation (Kőhler, 1936). The studies on chemical composition of fog droplets suggested that the SO_4^{2-}, NO_3^-, NH_4^+, and Cl^- were the major components of soluble saline ions of fog droplets (Fahey et al., 2005; Li et al., 2011b). For aerosol particle size smaller than 1 μm (PM_1) in Beijing, the mass of nitrate, sulfate, and ammonium accounted for about 37% of total aerosol mass, and that of organic matter was about 40% (Zhang et al., 2012). With the increase of understanding of aerosol chemical properties, the multi-component particles containing soluble and slightly soluble aerosol particles and soluble gases were taken into account for aerosol hygroscopic growth in the modified Kőhler equation (Petters et al., 2007; Laaksonen et al., 1998).

In an attempt to analyze activation of aerosol to CCN and the conversion of CCN to fog droplet, we calculated the ratios of activation and conversation based on the observed number concentration of aerosols, CCN and fog droplets (N_p, N_{CCN} and N_d). Since the CCN denotes the activated aerosols as fog droplet condensation nucleus at a given supersaturation, which is not the actual activated aerosols at environment, it can be used to assess the transform ability from aerosols to fog droplets. The ratio for aerosol activation to CCN and that for CCN conversion to fog droplets are denoted by activation ratio and conversation ratio, respectively, and are defined as follows:

$$\text{Acvtivation ratio} = N_{CCN}/N_p \times 100\%, \quad (1)$$

$$\text{Conversation ratio} = N_d/N_{CCN} \times 100\%, \quad (2)$$

where N_p and N_d are observed number concentrations of aerosols and fog droplets, and N_{CCN} is the number concentration of CCN.

Aerosols with size below 50 nm are too small to activate, so that the aerosols less than 50 nm are negligible in the calculation of activation ratio and conversation ratio at supersaturation of 0.2% and 0.4%. Gerber (1991) measured RH with light-reflecting substrate of a dewpoint hygrometer, and obtained the RH range with 100±0.4% during the period of fog event in Albany county. Figure 11 shows the temporal variations of activation ratio and conversation ratio at supersaturation of 0.2% and 0.4%. Figure 11(a) indicates that the activation ratio was almost smaller than 5% beyond the explosive activation period, which was much less than that in the cloud observed by aircraft (Lu et al., 2012). This is due to the fact that the instruments for aerosols used in two filed studies were different. The detectable largest particle size of SMPS used in this study is 0.661 μm, and that the airborne PCASP-100X used in cloud observation has size ranging between 0.1 and 3.0 μm. The small-size aerosols are usually much more than larger-size ones in atmosphere, so that the number concentration of aerosols in this study is much high. Rangognio et al. (2009) pointed out that when aerosol number concentration was set to be 8300 cm^{-3} without including the aerosols less than 50 nm based on the SMPS data in Paris fog study, the simulated CCN activation ratio was less than 5% with modified Kőhler equation in which the $(NH_4)_2SO_4$, NH_4NO_3, and organic material were considered as the major component of aerosols. In our study, the number concentration of aerosols was much larger than 8300 cm^{-3}, and the calculated activation ratio from observed data was also less than 5%. However,

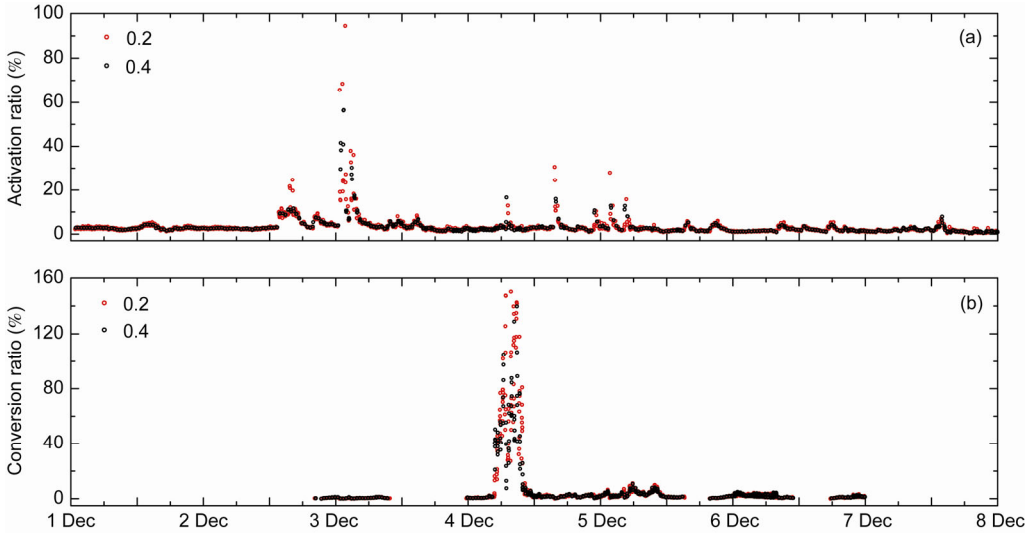

Figure 11 Activation ratio of CCN (a) and conversation ratio of fog droplet (b) at the supersaturation (ss) of 0.2% and 0.4% respectively in the second process.

the simulated results could not reflect the explosive activation phenomenon during heavy fog periods. The activation ratio reached 17% at supersaturation of 0.4% at about 07∶00 on 4 December and 30% at supersaturation of 0.2% at about 16∶00. The high activation ratio appeared three times from 00∶00 to 06∶00 on 5 December. The high activation ratio at 07∶00 on 4 December and that on 5 December corresponded well with the enhanced development of fog and also that from the afternoon of 2 December to the morning of 3 December. This illustrated that under the condition of strong cooling and favorable environmental supersaturation, the explosive activation of aerosols could promote the development of fog. But the high activation ratio at 16∶00 on 4 December corresponded to the weak period of fog intensity due to the warmer environment.

The conversion ratio from CCN to fog droplet can reflect that how many aerosols are converted to fog droplets in the transition stage. The temporal variation of conversion ratio in Figure 11(b) shows that the conversion ratio increased first and then decreased during the period between 05∶00 and 10∶00 on 4 December, and corresponded well with the mature stage of fog formation. The peak of conversation ratio reached 150%, indicating that there was very high conversion efficiency from CCN to fog droplets. The reason for conversion ratio larger than 100% is possibly due to that there was a temporal and spatial difference for CCN accumulation and explosive development of fog in an open atmospheric environment. As long as the actual supersaturation reached the given one, the CCN measured should be converted into fog droplets completely. Therefore, the explosive activation of haze aerosols in accumulation mode supplied enough large-size CCN, which lowered the supersaturation needed for condensational growth, greatly shortened the condensational growth time of fog droplets, and broadened the fog droplet spectrum rapidly.

3 Discussion and conclusions

We studied the synoptic pattern, boundary layer structure, microphysical properties of aerosols and fog, and the characteristics and mechanism of formation, evolution, and transition of a fog and haze episode lasted for one week on 1–7 December, 2011. The main conclusions are summarized as follows:

(1) The long-lasting fog and haze episode for one week could be divided into three main processes from its variation and intensity, and each process could include three main stages based on physical properties: haze aerosol accumulation, transition and mixture, and dissipation. The formation and development of the fog and haze event was closely related to the variation of synoptic pattern and boundary layer structure.

(2) The fog and haze event had different generation mechanism and features. The first process of fog and haze weather on 1–2 December was produced by radiation cooling and advection, and then weakened by a weak cold front at 08∶00 on 3 December; the second process on 3–4 December was caused initially by temperature inversion due to radiative cooling, and enhanced and developed on 5 December due to the influence of southerly warm and wet advection, and then weakened due to radiation heating. The third process was produced by both radiation cooling and warm and wet advection. The passage of a strong cold front terminated the long-lasting fog and haze process at about 12∶00 on 7 December.

(3) The haze aerosols accumulation stage occurred in the condition of temperature inversion, and was characterized by the increase of aerosol number concentration in Aitken nuclei mode and accumulation mode sequentially. When RH reached nearly 100%, haze aerosols started to be transformed into fog droplets in the transition and mixture stage. The release of latent heating produced by fog droplet condensational process and the high number concentration of haze aerosols intensified Brownian coagulation process and induced the size of aerosols to shift from smaller size to larger one, and provided appropriate size aerosols that can be effectively activated to CCN. Under strong cooling and high humid conditions the explosive activation of CCN enhanced the fog and haze mixture and development. The weak precipitation process during the fog and haze event had an obvious role in washout and scavenging on aerosols. The ratio of aerosol activated to CCN was lower than 5% in general period, but in the explosive period it reached 17%. The ratio of CCN converted to fog droplet exceeded 100%, showing an explosively broadening of fog droplet spectrum.

In this study, many data including aerosol concentration, LWC, RH, and horizontal visibility were used. On one hand, the LWC data unavailable in conventional observation can be used to quantitatively examine the intensity of fog. On the other hand, the combination of data for haze aerosols content, horizontal visibility, and RH could make the identification and transformation of haze and fog more objective. The results from this study suggested that in the aerosol accumulation stage the aerosol particles were accumulated abundantly and resulted in the increase of N_p and M_p, but LWC was very low, and ranged from 0 to 10^{-5} g m^{-3}. In the transition and mixture stage, N_p dropped sharply, but M_p remained at a high value, and LWC increased to 10^{-4} g m^{-3}. The RH at surface reached 100%. However, there were also transient oscillations in which LWC was less than 10^{-4} g m^{-3} and RH was smaller 100%, and it is attributed to the mixture of mist and haze. In the dissipation stage, LWC remained an order of 10^{-5} g m^{-3} but continued to decline, RH was smaller than 100%, and M_p declined slightly.

In addition, the activation ratio of aerosol to CCN and conversion ratio of CCN to fog droplet were also investigated, which has important application in quantitative estimation of the effect of polluted aerosols on the formation

and evolution of fog and haze. The classifications of haze aerosols accumulation, transition and mixture, and dissipation stages were based mainly on the observed physical features of the fog and haze event. The investigation of microphysical properties of haze to fog is important to understand the interactions between haze and fog as well as the formation mechanism.

This work was supported by the National Meteorology Public Welfare Industry Research Project (Grant No. GYHY200806001), the Program for Postgraduates Research Innovation of Jiangsu Higher Education Institutions (Grant No. CXZZ13-0511) and the Special Foundation of Chinese Academy of Meteorological Sciences (Grant No. 2011Z005).

China Meteorological Administration. 2003. Specifications for Surface Meteorological Observation (in Chinese). 2nd ed. Beijing: China Meteorological Press. 24–25

China Meteorological Administration. 2010. Observation and forecasting levels of haze. The State Standard of the People's Republic of China QX/T 113-2010 (in Chinese). Beijing: China Meteorological Press

Dall'Osto M, Harrison R M, Coe H, et al. 2009. Real-time secondary aerosol formation during a fog event in London. Atmos Chem Phys, 9: 2459–2469

Drewnick F, Jayne J T, Canagaratna M, et al. 2004. Measurement of ambient aerosol composition during the PMTACS-NY 2001 using an aerosol mass spectrometer. Part II: Chemically speciated mass distributions. Aerosol Sci Tech, 38:104–117

Eldridge R G. 1969. Mist-the transition from haze to fog. Bull Amer Meteorol Soc, 50: 422–426

Elias T, Haeffelin M, Drobinski P, et al. 2009. Particulate contribution to extinction of visible radiation: Pollution, haze, and fog. Atmos Res, 92: 443–454

Fahey K M, Pandis S N, Colett Jr J L, et al. 2005. The influence of size-dependent droplet composition on pollutant processing by fogs. Atmos Environ, 39: 4561–4574

Friedlander S K. Smoke, Dust, and Haze: Fundamentals of Aerosol Dynamics. 2nd ed. New York: Oxford University Press. 188–219

Gautam R, Hsu N C, Kafatos M, et al. 2007. Influences of winter haze on fog/low cloud over the Indo-Gangetic. J Geophys Res, 112: 207–218

Gerber H E. 1981. Microstructure of a radiation fog. J Atmos Sci, 38: 454–458

Gerber H. 1991. Supersaturation and droplet spectral evolution in fog. J Atmos Sci, 48: 2569–2588

Gultepe I, Tardif R, Michaelides S C, et al. 2007. Fog research: A review of past achievements and future perspectives. Pure Appl Geophys, 164: 1121–1159

Heintzenberg J. 1989. Fine particles in the global troposphere A review. Tellus Ser B-Chem Phys Meteorol, 41: 149–160

Hudson J G. 1980. Relationship between fog condensation nuclei and fog microstructure. J Atmos Sci, 37: 1854–1867

Husar R B, Whitby K T, Liu B Y H. 1972. Physical mechanisms governing the dynamics of Los Angeles smog aerosol. J Colloid Interface Sci, 39: 211–224

Husar R B, Holloway J M. 1984. The properties and climate of atmospheric haze. Hygroscopic Aerosols, Hampton Virginia: A Deepak Publishing. 129–170

Jacobson M Z. 1997. Development and application of a new air pollution modeling system-II. Aerosol module structure and design. Atmos Environ, 31: 131–144

Jia X C, Guo X L. 2012. Impacts of anthropogenic atmospheric pollutant on formation and development of a winter heavy fog event (in Chinese). Chin J Atmos Sci, 36: 995–1008

Kang H Q, Zhu B, Su J F, et al. 2013. Analysis of a long-lasting haze episode in Nanjing, China. Atmos Res, 120–121: 78–87

Köhler H. 1936. The nucleus in and the growth of hygroscopic droplets. Trans Faraday Soc, 32: 1152–1161

Laaksonen A, Korhonen P, Kulmala M, et al. 1998. Modification of the Kőhler equation to include soluble trace gases and slightly soluble substances. J Atmos Sci, 55: 853–862

Lewis J, Koracin D, Rabin R, et al. 2003. Sea fog off the California coast: Viewed in the context of transient weather systems. J Geophys Res, 108: 4457

Li Z H, Peng G Z. 1994. Physical and chemical characteristics of the Chongqing winter fog (in Chinese). Acta Meteorol Sin, 52: 477–483

Li Z H, Liu D Y, Yang J. 2011a. The microphysical processes and macroscopic condition of the radiation fog droplet spectrum broadening (in Chinese). Chin J Atmos Sci, 35: 1–14

Li Z H, Liu D Y, Feng Y, et al. 2011b. Recent progress in the studies of the fog-water chemical characteristics in China (in Chinese). Acta Meteorol Sin, 69: 544–554

Liu D Y, Pu M J, Yang J, et al. 2010. Microphysical structure and evolution of a four-day persistent fog event in Nanjing in December 2006. Acta Meteorol Sin, 24: 104–115

Liu X G, Li J, Qu Y, et al. 2013. Formation and evolution mechanism of regional haze: A case study in the megacity Beijing, China. Atmos Chem Phys, 13: 4501–4514

Lu G X, Guo X L. 2012. Distribution and origin of aerosol and its transform relationship with CCN derived from the spring multi-aircraft measurements of Beijing Cloud Experiment (BCE). Chin Sci Bull, 57: 2460–2469

Meng Z Y, Dabdub D, Seinfeld J H. 1998. Size-resolved and chemically resolved model of atmospheric aerosol dynamics. J Geophys Res, 103: 3419–3435.

Meyer M B, Jiusto J E, Garland L G. 1980. Measurements of visual range and radiation fog (haze) microphysics. J Atmos Sci, 37: 622–629

Meteorological Office. 1994. Handbook of Aviation Meteorology. 3rd ed. London: His Majesty's Stationery Office

Niu S J, Lu C S, Yu H Y, et al. 2010. Fog research in China: An overview. Adv Atmos Sci, 27: 639–661

Ogren J A, Noone K J, Hallberg A, et al. 1992. Measurement of the size dependence of the concentration of non-volatile material in fog droplets. Tellus Ser B-Chem Phys Meteorol, 44: 570–580

Pandis S N, Seinfeld J H, Pilinis C. 1990. The smog-fog-smog cycle and acid deposition. J Geophys Res, 95: 18489–18500

Petters M D, Kreidenweis S M. 2007. A single parameter representation of hygroscopic growth and cloud condensation nucleus activity. Atmos Chem Phys, 7: 1961–1971

Pinnick R G, Hoihjelle D L, Fernandez G, et al. 1978. Vertical structure in atmospheric fog and haze and its effects on visible and infrared extinction. J Atmos Sci, 35: 2020–2032

Podzimek J. 1997. Droplet concentration and size distribution in haze and fog. Stud Geophys Geod, 41: 277–296

Podzimek J. 1998. Aerosol particle scavenging by fog and haze droplets. Stud Geophys Geod, 42: 540–560

Pu M J, Zhang G Z, Yan W L, et al. 2008. Features of a rare advection-radiation fog event. Sci China Ser D-Earth Sci, 51: 1044– 1052

Quan J, Zhang Q, He H, et al. 2011. Analysis of the formation of fog and haze in North China Plain (NCP). Atmos Chem Phys, 11: 8205–8214

Rangognio J, Tulet P, Bergot T, et al. 2009. Influence of aerosols on the formation and development of radiation fog. Atmos Chem Phys Discuss, 9: 17963–18019

Remer L A, Tanre D, Kaufman Y J. 2006. Algorithm for Remote Sensing of Tropospheric Aerosol from MODIS: Collection 005. Product ID: MOD04/MYD04. Algorithun Theoretical Basis Document. National Aeronautics and Space Administration

Seinfeld J H, Pandis S N. 1997. Atmospheric Chemistry and Physics: From Air Pollution to Climate Change. New York: John Wiley and Sons. 377–390

Stein D C, Swap R J, Greco S, et al. 2003. Haze layer characterization and associated meteorological controls along the eastern coastal region of southern Africa. J Geophys Res, 108: 8506

Stewart R E, Yiu D T, Chung K K, et al. 1995. Weather conditions associated with the passage of precipitation type transition regions over eastern Newfoundland. Atmos-Ocean, 33: 25–53

Tang X Y, Zhang Y H, Shao M, et al. 2006. Atmospheric Environmental Chemistry (in Chinese). 2nd ed. Beijing: Higher Education Press. 286–290
Wang X F, Wang W X, Yang L X, et al. 2012. The secondary formation of inorganic aerosols in the droplet mode through heterogeneous aqueous reactions under haze conditions. Atmos Environ, 63: 68–76
WMO/GAW. 2003. WMO/GAW Aerosol Measurement Procedures Guidelines and Recommendations. WMO TD No-1178-GAW Report No.153. World Meteorological Organization, Geneva
WMO. 2005. Aerodrome Reports and Forecasts: A User's Handbook to the Codes. WMO No.782. World Meteorological Organization, Geneva
Wu D, Tie X X, Li C C, et al. 2005. An extremely low visibility event over the Guangzhou region: A case study. Atmos Environ, 39: 6568–6577
Yang J, Niu Z Q, Shi C E, et al. 2010. Microphysics of atmospheric aerosols during winter haze/fog events in Nanjing (in Chinese). Environ Sci, 31: 1425–1431
Yu X N, Zhu B, Yin Y, et al. 2011. A comparative analysis of aerosol properties in dust and haze-fog days in a Chinese urban region. Atmos Res, 99: 241–247
Zhang Q, Tie X X, Lin W L, et al. 2013. Variability of SO_2 in an intensive fog in North China Plain: Evidence of high solubility of SO_2. Particuology, 11: 41–47
Zhang X Y, Zhang Y M, Cao G L. 2012. Aerosol chemical compositions of Beijing PM1 and its control countermeasures (in Chinese). J Appl Meteorol Sci, 23: 257–264